PERGAMON

International Journal of Heat and Mass Transfer 44 (2001) 2011–2027

International Journal of HEAT and MASS TRANSFER

www.elsevier.com/locate/ijhmt

Solution of inverse free convection problems by conjugate gradient method: effects of Rayleigh number

M. Prud'homme, T. Hung Nguyen *

Department of Mechanical Engineering, École Polytechnique de Montréal, C.P. 6079, Succ. Centre-ville, Montréal, Québec, Canada H3C 3A7

Received 31 August 1999; received in revised form 16 August 2000

Abstract

A study is made of the inverse free convection problem (IFCP) by adjoint equations and conjugate gradient (CG), to determine an unknown space and time dependent boundary heat flux on the side of an enclosure, from temperature measurements by sensors within the flow. The direct, sensitivity and adjoint set of equations for a Boussinesq fluid are solved by control volumes. Solutions are presented for different types of boundary conditions and a wide range of Rayleigh numbers, for a square enclosure. It is found that by placing sensors close enough to the active boundary, solutions may be achieved for Rayleigh numbers higher than in previous studies. Noisy data solutions are regularized by stopping the iterations according to the discrepancy principle of Alifanov, before the high frequency components of the random noises are reproduced. The accuracy of the solutions is shown to depend strongly on the Rayleigh number, the sensor's position and the type of boundary conditions imposed.

1. Introduction

Inverse heat transfer problems are encountered in many situations where the direct measurement of boundary conditions or the determination of thermophysical properties of a system are impracticable. A typical inverse heat conduction problem (IHCP) consists of estimating the temperature or heat flux on the part of the boundary surface of a body, through the use of remote temperature measurements taken either within the body itself or on a different part of the bounding surface. In direct problems, random errors of boundary value data used in the computation of a temperature within the body are damped by diffusion, while in inverse problems errors arising from internal measurements are amplified when the unknown boundary values are estimated. Thus a small error in the input data can lead to a large error in the inverse solution. The inverse problem is consequently regarded as an ill-posed one from a mathematical point of view, in the sense of Hadamard [1].

A lot of research has been conducted over the last decades, to devise ways to reduce the effect of error growth in IHCP solutions. Since the problem is not well posed, a direct solution procedure requiring exact matching of the calculated temperatures with the measured data is unstable. Some improvement in stability is possible by using a least-squares method [2,3] seeking to minimize the error between the calculated and measured temperatures. The procedure is simple and accurate for exact data, but the solutions are prone to instability with inaccurate data.

To regularize the problem, a technique described by Tikhonov and Arsenin [4] can be used, which modifies the least-squares method by adding a smoothing constraint term, multiplied by an appropriate regularization parameter. The success of the technique depends on the choice of the regularization parameter however, which is not always easy to make in practical calculations. The so-called iterative regularization method described by Alifanov [5] provides an alternative to the Tikhonov procedure. Both procedures may be classified among the

* Corresponding author. Tel.: +514-340-4711; fax: +514-340-5917.

E-mail address: miprud@meca.polymtl.ca (T. Hung Nguyen).

0017-9310/01/$ - see front matter
PII: S0017-9310(00)00266-0

Nomenclature

C	boundary
c_p	specific heat
g	gravity
H	height
k	thermal conductivity
p	conjugate search direction
Pr	Prandtl number
q	heat flux
Q_{ref}	reference flux value
Ra	Rayleigh number
S	surface
t	time
T	temperature
$\boldsymbol{u}$	velocity vector
x, y	coordinates

Greek symbols

α	step size
β	coefficient of thermal expansion
δ	Dirac delta function
Δ	increment
ε	small number
ν	kinematic viscosity
σ	standard deviation
ρ	density
ψ	stream function
ω	vorticity

Superscripts

k	iteration number
$*$	active boundary
$\sim$	sensitivity variable
$\bar{}$	adjoint variable
$\wedge$	unit vector

Subscripts

m	measurement value
0	reference value
f	final value

Other symbols

$\langle \cdot \vert \cdot \rangle$	inner product
$\Vert \cdot \Vert$	norm
∇	gradient
$\nabla_n \times$	normal component of curl

whole domain methods, in which the unknown heat flux is determined at once for all times and/or positions. These methods are based on sound mathematical background and may be applied to a great variety of inverse problems. Other methods were also developed over the years, for instance the maximum entropy method [6], the minimal energy method [7], the mollification method [8], the space marching [9] and random search methods [10].

The approach of Beck [11,12], also referred to as the function specification method, is probably the best known sequential method for IHCPs, where the time domain is subdivided and the least-squares problem solved over each subdomain in sequence, using assumptions about future data for stabilization. The stability of the Beck's method was analyzed by Liu [13], and Reinhardt [14] extended it to two-dimensional problems. A comparison of the function specification method with the whole domain methods was made by Beck et al. [15] who showed that the Tikhonov method, the iterative regularization method (also referred to as the conjugate gradient (CG) method) and the function specification method give comparable results for the test problem considered. The optimal number of future times in Beck's method is problem-dependent and difficult to determine, just as the regularization parameter in the Tikhonov method or the number of iterations in the iterative regularization method.

While a great number of works focused on inverse *conduction* problems encountered in the design, control and identification of various thermal systems, much less were devoted to inverse heat transfer problems involving *convection flow*.

Convection heat transfer problems are governed by a system of partial differential equations, namely the continuity, Navier–Stokes, and energy equations. If we are dealing with a *forced convection* problem, the temperature field is obtained independently, by solving a single energy equation. Such a problem was solved by Huang and Özisik [16] for instance, to estimate the wall heat flux in a fully developed channel flow from temperature measurements inside the channel, using regular and modified CG methods. The case of a fully developed turbulent channel flow was considered by Liu and Özisik [17], who used the same approach to determine the time-varying wall heat flux. The estimation of the temperature profile at the entrance of a thermally developing, hydrodynamically developed flow between parallel plates was considered by Ramanujam [18], while the estimation of the time-varying inlet temperature in laminar flow in a parallel plate duct was presented by Bokar and Özisik [19]. The thermal conductivity and heat capacity of forced flow inside a circular duct were determined from transient temperature at a single location in the downstream region by Liu and Özisik [20], using the Levenberg–Marquardt method. Recently, Hsu et al. [21] presented a two-dimensional inverse least-squares method to estimate both inlet temperature and wall heat flux in a steady laminar flow in a circular duct.

Inverse *natural convection* problems are more difficult to investigate than forced convection problems, as the temperature and flow field are always coupled. Moutsoglou [22] solved by the sequential function specification method a steady laminar inverse natural convection in a vertical channel, where the heat flux at one wall is unknown while the temperature on the opposite insulated wall is given. More recently, Park and Chung [23] solved the inverse problem for an unknown time-dependent heat source inside a square cavity, using the Chebyshev pseudospectral method. The same problem was considered by Park and Jung [24], using the Karhunen–Loève Galerkin method to solve the set of direct, adjoint and sensitivity equations. This method was shown to be as accurate as the pseudospectral method, but at a "drastically reduced" cost in computer time. Zabaras and Yang [25] and Yang and Zabaras [26] used finite element method, in conjunction with CG technique to solve inverse problems involving natural convection. Nguyen [27] and Prud'homme and Nguyen [28] considered the inverse free convection problem (IFCP) in a square cavity with an unknown heat flux on one vertical wall, using data taken on the opposite wall. The results obtained were restricted to moderate Rayleigh numbers ranging between 0 and 10000. Satisfactory solutions could not be obtained for Rayleigh numbers greater than 10000.

In the present study, the effects of natural convection on the stability and accuracy of the inverse solution are analyzed in terms of the Rayleigh number and the sensor's position. It will be shown that, by moving sensors closer to the unknown boundary, stable solutions may be obtained for Rayleigh numbers higher than in the previous study [28]. In fact, if the unknown heat flux is strong enough for a boundary layer to develop, one should put sensors within that boundary layer.

The next section presents the detailed derivation of the sets of sensitivity and adjoint equations used in the CG technique. Numerical results will be presented next to show the effects of convection flow, sensor's location and boundary conditions on the convergence and accuracy of the inverse solutions.

2. Problem definition

Let us consider the general IFCP sketched in Fig. 1(a). Our purpose is to determine the unknown flux q on the active boundary C^* over the time interval $0 \leqslant t \leqslant t_\Gamma$, from temperature measurements T_m taken at the sensor's position. It will be assumed throughout the discussion that the boundary conditions (either temperatures or heat fluxes) are known on C, the remaining part of the boundary, and that the cavity is initially at temperature T_0 when heating begins. The IFCP may be expressed in a convenient non-dimensional form by introducing an appropriate scaling of the variables, based on the definitions

$$T^* = \frac{T - T_0}{\Delta T}, \quad \Delta T = \frac{Q_{\mathrm{ref}} H}{k}, \quad (x,y)^* = \frac{(x,y)}{H}, \quad t^* = \frac{kt}{\rho c_p H^2}, \tag{1}$$

where all properties are evaluated at T_0. Omitting superscripts from now on, the temperature, stream function and vorticity fields within the cavity satisfy the set of dimensionless equations

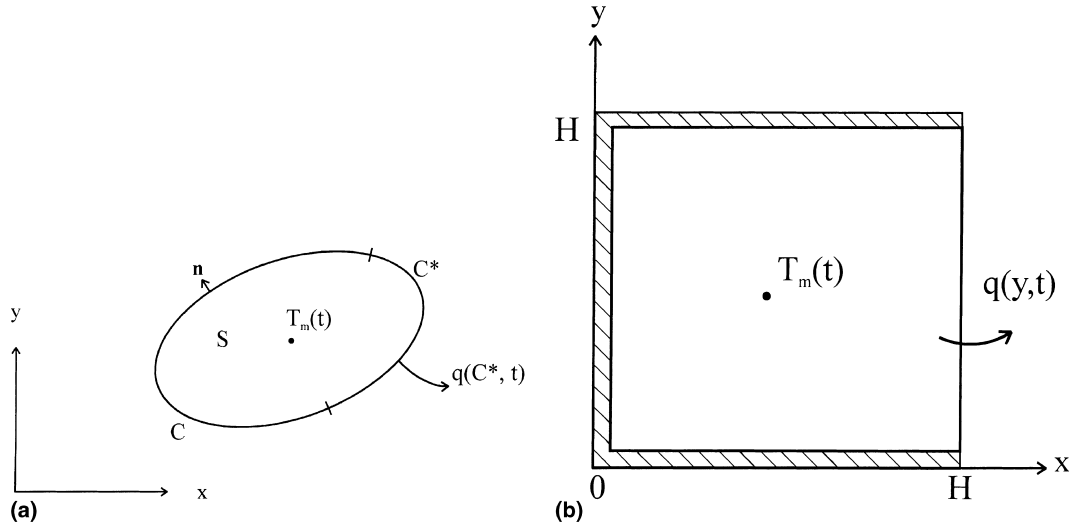

Fig. 1. (a) Solution domain for general formulation; (b) geometry and coordinate system for test computations.

$$\frac{\mathrm{D}T}{\mathrm{D}t} = \nabla^2 T,$$
$$\frac{\mathrm{D}\omega}{\mathrm{D}t} = Pr\nabla^2\omega - RaPr\nabla_n \times (T\hat{\boldsymbol{g}}), \quad \nabla^2\psi = -\omega, \tag{2}$$

where $Ra = \rho c_p \beta g \Delta T H^3/kv$ is the Rayleigh number and $Pr = \rho c_p v/k$ is the Prandtl number. The corresponding boundary conditions are the usual no-slip requirement on C and C^* for the flow, and

$$-\frac{\partial T}{\partial n} = q \quad \text{on } C^*, \quad -\frac{\partial T}{\partial n} = f \quad \text{or } T = g \quad \text{on } C \tag{3}$$

for temperature, where f and g are known a priori and may be functions of position and time, just as q. In general, both Dirichlet and Neumann conditions can be considered simultaneously, on different parts of C.

In the inverse problem, we look for the boundary heat flux q that will minimize the error

$$E(q) = \frac{1}{2}\|T - T_m\|^2 \equiv \frac{1}{2}\int_0^{t_f} (T - T_m)^2 \,\mathrm{d}t, \tag{4}$$

where T and T_m are the predicted and given temperature at the sensor's position, respectively.

If q is a function of time only, not more than a single point sensor is needed to get a valid solution. For a non-uniform flux of arbitrary form, a continuum set of sensors is required in principle. But after discretization, it is enough to use a sensor at every computational point on an appropriate grid line inside the cavity. In this case, the error becomes the sum of individual contributions like the right-hand side of Eq. (4), taken at each sensor's location.

The minimization of the error can be achieved by iterative regularization, using the CG method. A sequence of approximations $q^0, q^1, \ldots q^k$, and so on is constructed for the unknown heat flux according to $q^{k+1} = q^k + \alpha^k p^k$. Here α^k is the step size and p^k the conjugate search direction, which is related to the gradient of E with respect to the function q, and may be determined according to a well-known algorithm [5,27,29]. The gradient of E and the step size α may be obtained, respectively, from the solution of the adjoint and sensitivity problems described below [27].

2.1. The sensitivity problem

Let us introduce the temperature sensitivity $\tilde{T}$ as the directional derivative of T at q in the direction Δq, i.e.,

$$\tilde{T} = \lim_{\varepsilon \to 0} \frac{T(q + \varepsilon\Delta q) - T(q)}{\varepsilon} \tag{5}$$

and so on for the other two variables. Based on this definition, it is straightforward to derive from Eq. (2) that the temperature, vorticity and stream function sensitivity fields are solutions of

$$\frac{\partial \tilde{T}}{\partial t} + \nabla \cdot \left(\boldsymbol{u}\tilde{T} + \tilde{\boldsymbol{u}}T\right) = \nabla^2 \tilde{T},$$
$$\frac{\partial \tilde{\omega}}{\partial t} + \nabla \cdot \left(\boldsymbol{u}\tilde{\omega} + \tilde{\boldsymbol{u}}\omega\right) = Pr\nabla^2\tilde{\omega} - RaPr\nabla_n \times (\tilde{T}\hat{\boldsymbol{g}}),$$
$$\nabla^2\tilde{\psi} = -\tilde{\omega}. \tag{6}$$

It is further shown that the vorticity and stream function sensitivities must verify the same initial and boundary conditions as their direct problem counterparts. The temperature sensitivity is expected to satisfy the initial condition $\tilde{T} = 0$, with the boundary conditions

$$-\frac{\partial \tilde{T}}{\partial n} = \Delta q \quad \text{on } C^*, \quad -\frac{\partial \tilde{T}}{\partial n} = 0 \quad \text{or } \tilde{T} = 0 \quad \text{on } C. \tag{7}$$

2.2. The adjoint problem

In an infinite-dimensional space, the gradient of E, designated by ∇E, must verify the formal equality

$$D_{\Delta q}E(q) = \langle \nabla E | \Delta q \rangle, \tag{8}$$

where the left-hand side is the directional derivative of E at q in the direction Δq. The gradient of E may then be determined by a set of adjoint equations as follows. The derivation will be done in the case of a single sensor for

Table 1
Test cases considered

Case	Bc at $x = 0$	Unknown flux	Rayleigh number	Sensor position
1	Adiabatic	$q = \sin(2\pi t)$	0	$x = 0.00, 0.50$
2	Adiabatic	$q = \sin(2\pi t)$	10^3	$x = 0.00, 0.50$
3	Adiabatic	$q = \sin(2\pi t)$	10^4	$x = 0.25, 0.75$
4	Adiabatic	$q = \sin(2\pi t)$	10^5	$x = 0.50, 0.75$
5	Adiabatic	Triangular profile	10^5	$x = 0.75, 0.90$
6	Adiabatic	Step profile	10^5	$x = 0.75, 0.90$
7	Adiabatic	$q = \sin(2\pi t)\sin(\pi y)$	10^5	$x = 0.90$
8	Isothermal	$q = \sin(2\pi t)$	10^6	$x = 0.50, 0.75$

the sake of clarity. Starting from Eq. (4), the directional derivative of E is

$$D_{\Delta q}E(q) = \left\langle T - T_{\mathrm{m}} | \tilde{T} \right\rangle \equiv \int_0^{t_{\mathrm{f}}} (T - T_{\mathrm{m}})\tilde{T}\,\mathrm{d}t, \tag{9}$$

where all quantities are evaluated at the sensor's location. If many sensors are involved, a sum of such integrals is involved, but the steps of the derivation are the same. Let us introduce the so-called adjoint temperature $\overline{T}$, vorticity $\overline{\omega}$, stream function $\overline{\psi}$ and note that the right-hand side of Eq. (9) may be expressed equivalently as an integral over surface and time using Dirac's delta function. Substituting Eq. (6) in Eq. (9), we may write

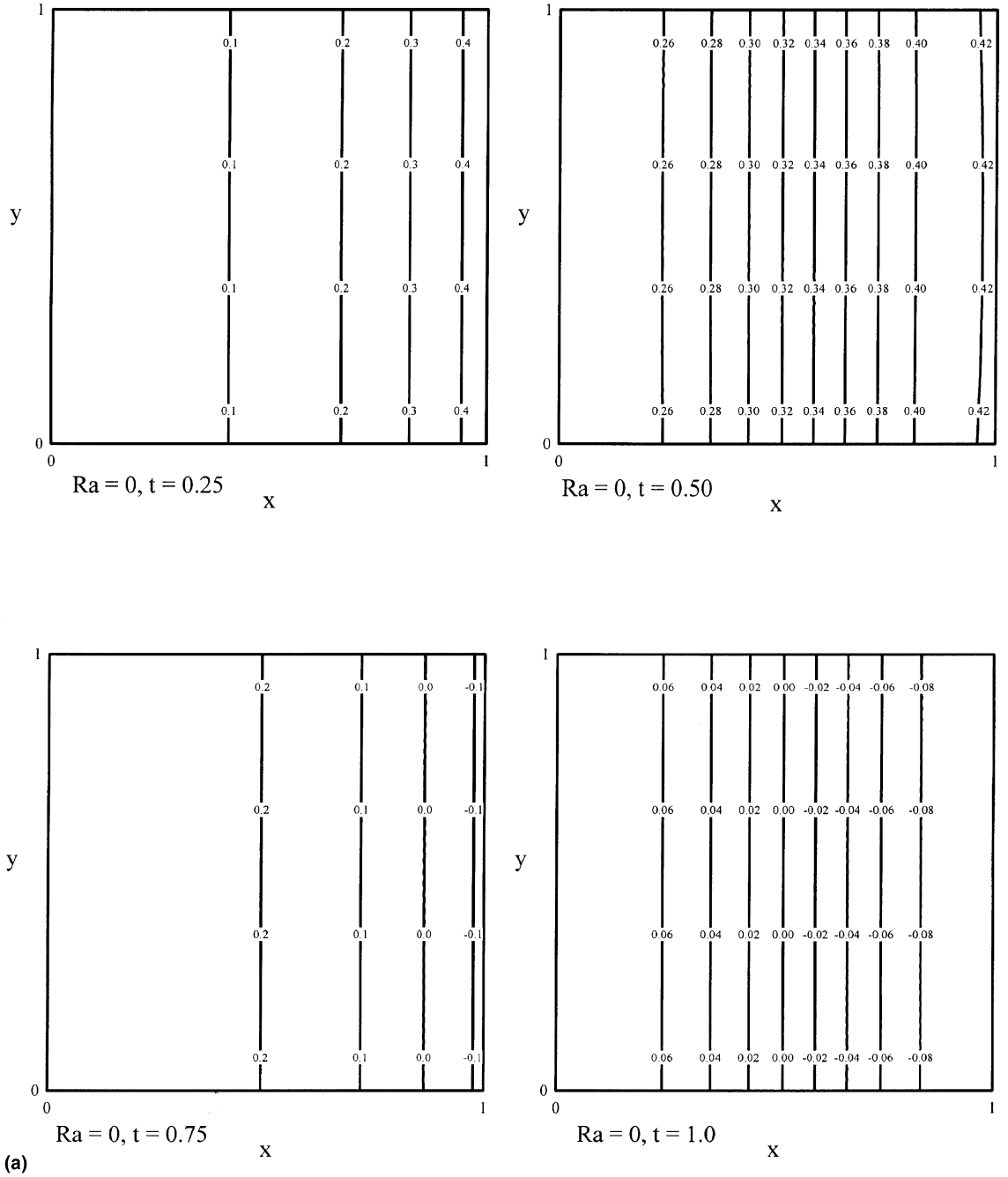

Fig. 2. (a) Isotherms, direct problem, $q(t) = -\sin(2\pi t)$, $Ra = 0$; (b) flux prediction, $q(t) = -\sin(2\pi t)$, $Ra = 0$.

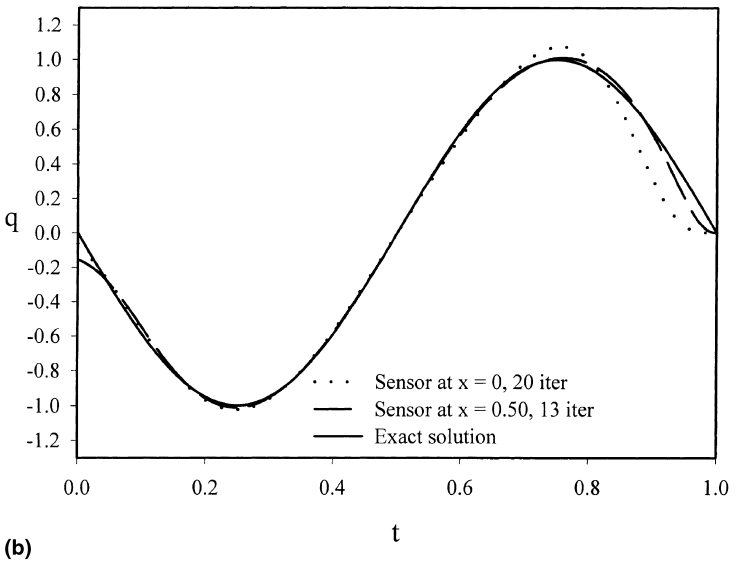

Fig. 2 (*continued*)

$$
\begin{aligned}
D_{\Delta q}E(q) = & \int_0^{t_f}\int_S (T-T_m)\tilde{T}\delta(\boldsymbol{r}-\boldsymbol{r}_m)\,\mathrm{d}S\,\mathrm{d}t \\
& + \int_0^{t_f}\int_S \overline{\psi}\left\{\nabla^2\tilde{\psi}+\tilde{\omega}\right\}\mathrm{d}S\,\mathrm{d}t \\
& + \int_0^{t_f}\int_S \overline{\omega}\left\{\frac{\partial\tilde{\omega}}{\partial t}+\nabla\cdot\left(\boldsymbol{u}\tilde{\omega}+\tilde{\boldsymbol{u}}\omega\right)\right. \\
& \left. - Pr\nabla^2\tilde{\omega}+RaPr\nabla_n\times(\tilde{T}\hat{\boldsymbol{g}})\right\}\mathrm{d}S\,\mathrm{d}t \\
& + \int_0^{t_f}\int_S \overline{T}\left\{\frac{\partial\tilde{T}}{\partial t}+\nabla\cdot\left(\boldsymbol{u}\tilde{T}+\tilde{\boldsymbol{u}}T\right)\right. \\
& \left. - \nabla^2\tilde{T}\right\}\mathrm{d}S\,\mathrm{d}t. \qquad (10)
\end{aligned}
$$

By virtue of the Green's identities and the divergence theorem, and the no-slip condition at the boundary, it follows from Eq. (10) that

$$
\begin{aligned}
D_{\Delta q}E(q) = & \int_0^{t_f}\int_S (T-T_m)\tilde{T}\delta(\boldsymbol{r}-\boldsymbol{r}_m)\,\mathrm{d}S\,\mathrm{d}t \\
& + \int_0^{t_f}\int_S \left(\tilde{\psi}\nabla^2\overline{\psi}+\overline{\psi}\tilde{\omega}\right)\mathrm{d}S\,\mathrm{d}t \\
& + \int_0^{t_f}\int_S \left\{\overline{\omega}\frac{\partial\tilde{\omega}}{\partial t}-\tilde{\omega}(\boldsymbol{u}\cdot\nabla)\overline{\omega}-\omega(\tilde{\boldsymbol{u}}\cdot\nabla)\overline{\omega}\right. \\
& \left. - Pr\tilde{\omega}\nabla^2\overline{\omega}+RaPr\,\overline{\omega}\nabla_n\times(\tilde{T}\hat{\boldsymbol{g}})\right\}\mathrm{d}S\,\mathrm{d}t \\
& + \int_0^{t_f}\int_S \left\{\overline{T}\frac{\partial\tilde{T}}{\partial t}-\tilde{T}(\boldsymbol{u}\cdot\nabla)\overline{T}\right. \\
& \left. - T(\tilde{\boldsymbol{u}}\cdot\nabla)\overline{T}-\tilde{T}\nabla^2\overline{T}\right\}\mathrm{d}S\,\mathrm{d}t \\
& + \int_0^{t_f}\oint_{C+C^*}\left(\overline{\psi}\frac{\partial\tilde{\psi}}{\partial n}-\tilde{\psi}\frac{\partial\overline{\psi}}{\partial n}\right)\mathrm{d}l\,\mathrm{d}t \\
& - \int_0^{t_f}\oint_{C+C^*}\left(\overline{T}\frac{\partial\tilde{T}}{\partial n}-\tilde{T}\frac{\partial\overline{T}}{\partial n}\right)\mathrm{d}l\,\mathrm{d}t \\
& - Pr\int_0^{t_f}\oint_{C+C^*}\left(\overline{\omega}\frac{\partial\tilde{\omega}}{\partial n}-\tilde{\omega}\frac{\partial\overline{\omega}}{\partial n}\right)\mathrm{d}l\,\mathrm{d}t. \qquad (11)
\end{aligned}
$$

The first and the third boundary integrals on the right-hand side of Eq. (11) vanish on the assumption that the adjoint stream function, the adjoint vorticity and its normal derivative are equal to zero on C as well as C^*. Furthermore, if the adjoint temperature satisfies the condition

$$
-\frac{\partial\overline{T}}{\partial n}=0 \quad \text{on } C^*, \quad -\frac{\partial\overline{T}}{\partial n}=0 \quad \text{or } \overline{T}=0 \quad \text{on } C, \qquad (12)
$$

then the second boundary integral becomes using Eq. (7)

$$
\begin{aligned}
& -\int_0^{t_f}\oint_{C+C^*}\left(\overline{T}\frac{\partial\tilde{T}}{\partial n}-\tilde{T}\frac{\partial\overline{T}}{\partial n}\right)\mathrm{d}l\,\mathrm{d}t \\
& \quad = \int_0^{t_f}\int_{C^*}\overline{T}\Delta q\,\mathrm{d}l\,\mathrm{d}t. \qquad (13)
\end{aligned}
$$

Substituting Eq. (13) back into Eq. (11) using continuity gives, after a slight rearrangement of terms

$$
\begin{aligned}
D_{\Delta q}E(q) = & \int_0^{t_f}\int_S (T-T_m)\tilde{T}\delta(\boldsymbol{r}-\boldsymbol{r}_m)\,dS\,dt \\
& + \int_0^{t_f}\int_S \left(\tilde{\psi}\nabla^2\overline{\psi} + \overline{\psi}\tilde{\omega}\right)dS\,dt \\
& + \int_0^{t_f}\int_S \left\{\overline{\omega}\frac{\partial\tilde{\omega}}{\partial t} - \tilde{\omega}\nabla\cdot(\boldsymbol{u}\overline{\omega} + Pr\nabla\overline{\omega})\right. \\
& \left. + Ra\,Pr\,\overline{\omega}\nabla_n\times(\tilde{T}\hat{\boldsymbol{g}})\right\}dS\,dt \\
& + \int_0^{t_f}\int_S \left\{\overline{T}\frac{\partial\tilde{T}}{\partial t} - \tilde{T}\nabla\cdot(\boldsymbol{u}\overline{T} + \nabla\overline{T})\right\}dS\,dt \\
& + \int_0^{t_f}\int_{C^*} \overline{T}\Delta q\,dl\,dt \\
& - \int_0^{t_f}\int_S T(\tilde{\boldsymbol{u}}\cdot\nabla)\overline{T}\,dS\,dt \\
& - \int_0^{t_f}\int_S \omega(\tilde{\boldsymbol{u}}\cdot\nabla)\overline{\omega}\,dS\,dt \qquad (14)
\end{aligned}
$$

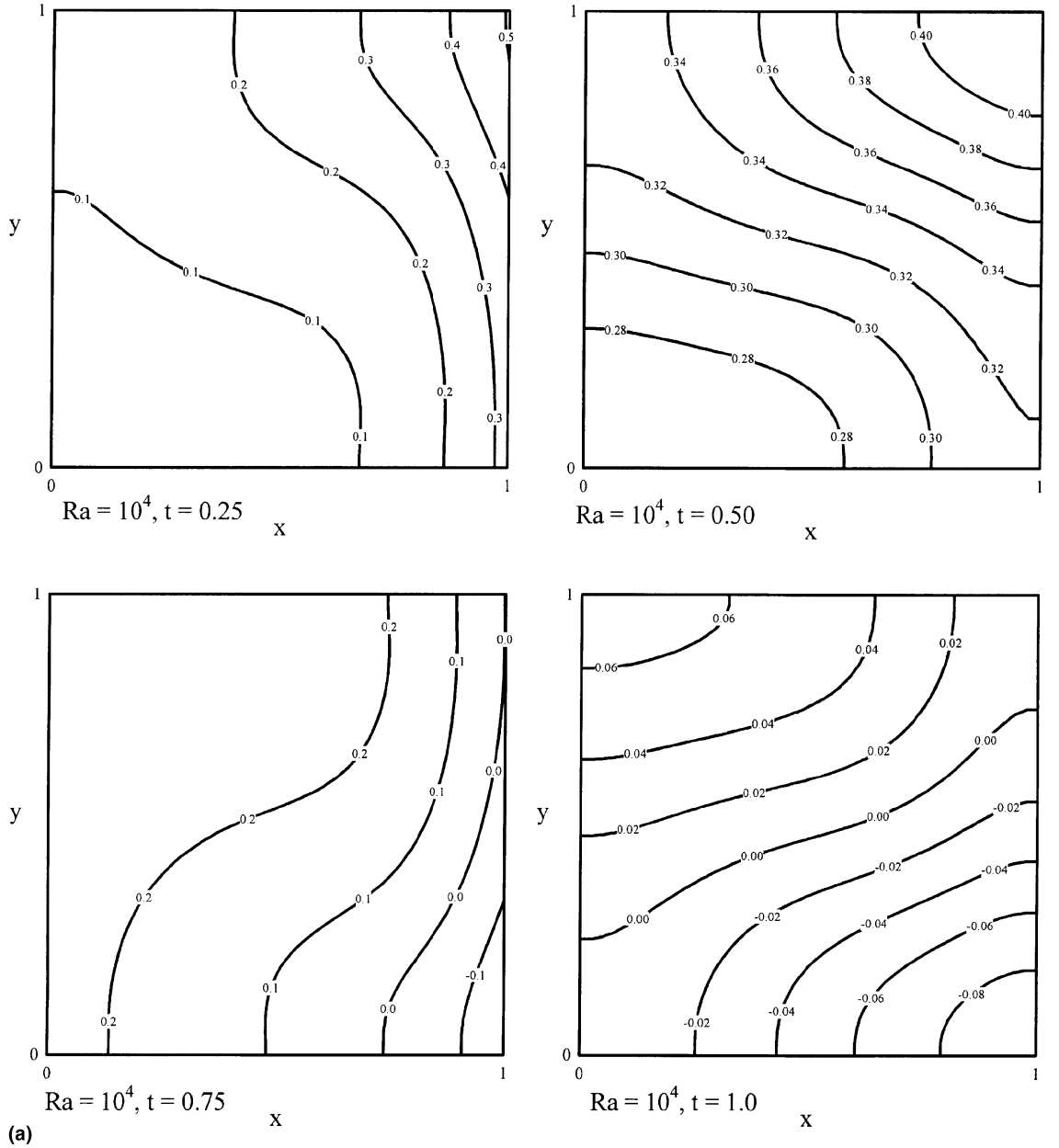

Fig. 3. (a) Isotherms, direct problem, $q(t) = -\sin(2\pi t)$, $Ra = 10^4$; (b) streamlines, direct problem, $q(t) = -\sin(2\pi t)$, $Ra = 10^4$; (c) flux prediction, $q(t) = -\sin(2\pi t)$, $Ra = 10^4$.

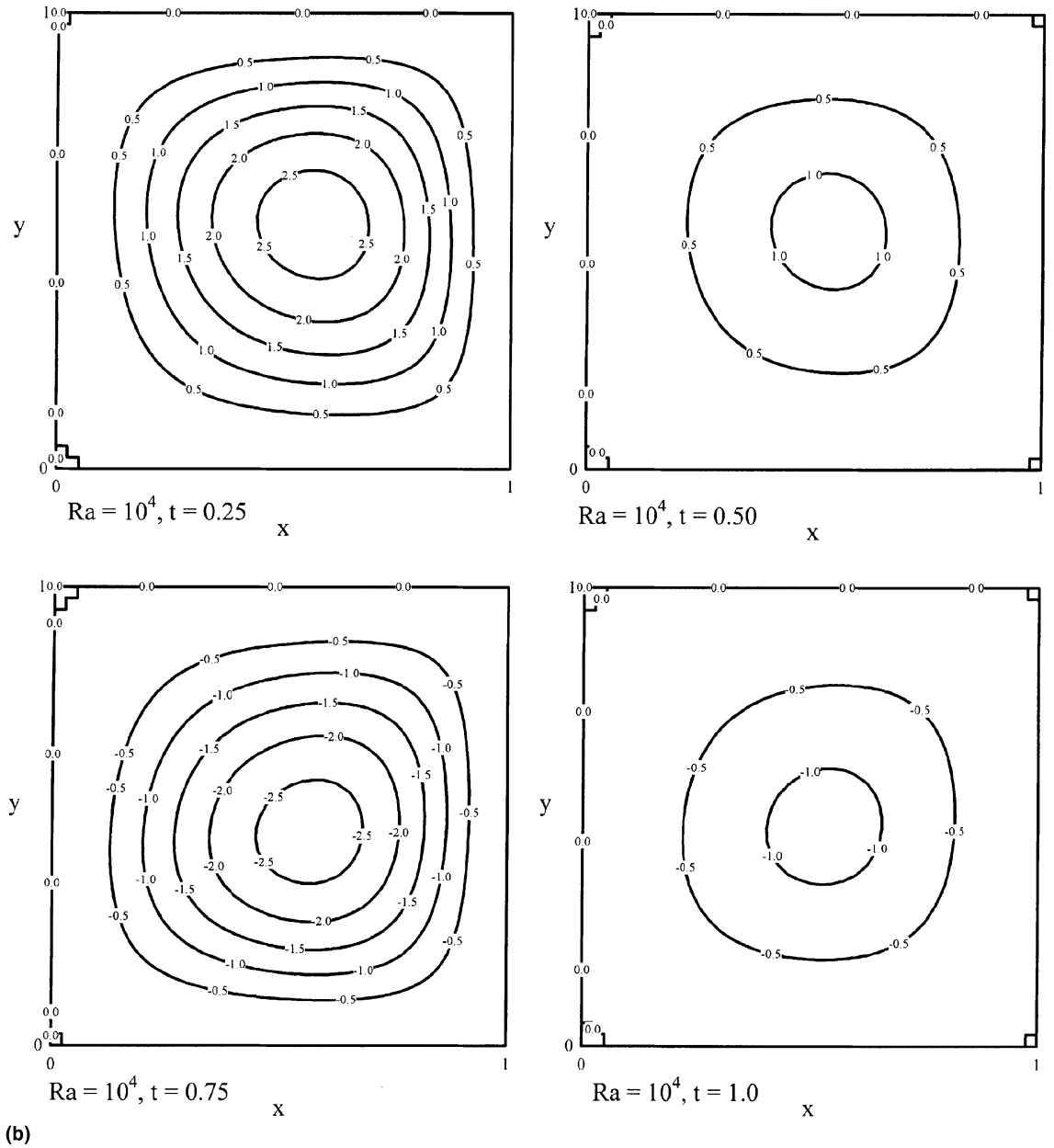

Fig. 3 (*continued*)

for the directional derivative. From the definition of the stream function, we have on the other hand

$$T(\tilde{u}\cdot\nabla)\overline{T} = -\nabla_n \times (T\tilde{\psi}\nabla\overline{T}) + \tilde{\psi}\frac{\partial(T,\overline{T})}{\partial(x,y)} \tag{15}$$

as can be verified by expanding both sides. This formula remains valid if temperatures are replaced by vorticities. Since gravity is a constant vector, it is straightforward to show that

$$\overline{\omega}\nabla_n \times \left(\tilde{T}\hat{\boldsymbol{g}}\right) = \nabla_n \times (\overline{\omega}\tilde{T}\hat{\boldsymbol{g}}) - \tilde{T}\nabla_n \times (\overline{\omega}\hat{\boldsymbol{g}}). \tag{16}$$

It follows from Eqs. (14)–(16), after using Green's theorem and the boundary condition on the adjoint vorticity, that

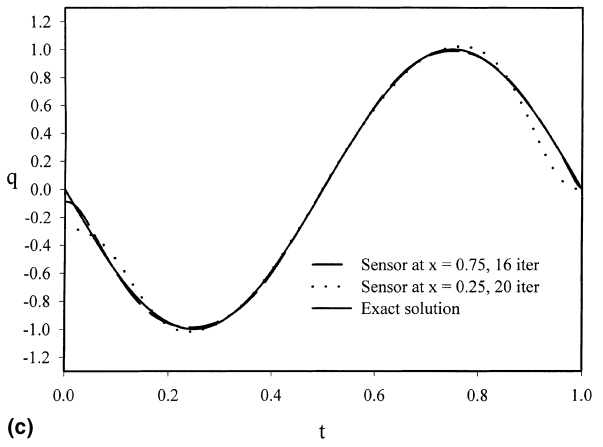

Fig. 3 (*continued*)

$$
\begin{aligned}
D_{\Delta q}E(q) = & \int_0^{t_f}\int_S (T-T_m)\tilde{T}\delta(\boldsymbol{r}-\boldsymbol{r}_m)\,dS\,dt \\
& + \int_0^{t_f}\int_S \tilde{\psi}\left\{\nabla^2\overline{\psi} - \frac{\partial(T,\overline{T})}{\partial(x,y)} - \frac{\partial(\omega,\overline{\omega})}{\partial(x,y)}\right\}dS\,dt + \int_0^{t_f}\int_S \left\{\overline{\omega}\frac{\partial\tilde{\omega}}{\partial t} - \tilde{\omega}\nabla\cdot(\boldsymbol{u}\overline{\omega} + Pr\nabla\overline{\omega}) + \overline{\psi}\tilde{\omega}\right\}dS\,dt \\
& + \int_0^{t_f}\int_S \left\{\overline{T}\frac{\partial\tilde{T}}{\partial t} - \tilde{T}\nabla\cdot(\boldsymbol{u}\overline{T} + \nabla\overline{T}) - Ra\,Pr\,\tilde{T}\nabla_n\times(\overline{\omega}\hat{\boldsymbol{g}})\right\}dS\,dt \\
& + \int_0^{t_f}\int_{C^*}\overline{T}\Delta q\,dl\,dt. \qquad (17)
\end{aligned}
$$

If the adjoint temperature and vorticity are both assumed to vanish at $t = t_f$, Eq. (17) can be simplified further as

$$
\begin{aligned}
D_{\Delta q}E(q) = & \int_0^{t_f}\int_S -\tilde{T}\left\{\frac{\partial\overline{T}}{\partial t} + \nabla\cdot(\boldsymbol{u}\overline{T} + \nabla\overline{T}) + Ra\,Pr\,\nabla_n\times(\overline{\omega}\hat{\boldsymbol{g}}) - (T-T_m)\delta(\boldsymbol{r}-\boldsymbol{r}_m)\right\}dS\,dt + \int_0^{t_f}\int_S -\tilde{\omega}\left\{\frac{\partial\overline{\omega}}{\partial t} + \nabla\cdot(\boldsymbol{u}\overline{\omega} + Pr\nabla\overline{\omega}) - \overline{\psi}\right\}dS\,dt \\
& + \int_0^{t_f}\int_S \tilde{\psi}\left\{\nabla^2\overline{\psi} - \frac{\partial(T,\overline{T})}{\partial(x,y)} - \frac{\partial(\omega,\overline{\omega})}{\partial(x,y)}\right\}dS\,dt + \int_0^{t_f}\int_{C^*}\overline{T}\Delta q\,dl\,dt \qquad (18)
\end{aligned}
$$

by interchanging the order of integration for the time derivatives and using the initial conditions of the sensitivity variables. All terms between brackets in Eq. (18) above vanish if the adjoint variables obey the set of equations

$$
\begin{aligned}
& \frac{\partial\overline{T}}{\partial t} + \nabla\cdot\left(\boldsymbol{u}\overline{T} + \nabla\overline{T}\right) + Ra\,Pr\,\nabla_n\times(\overline{\omega}\hat{\boldsymbol{g}}) \\
& \quad = (T-T_m)\delta(\boldsymbol{r}-\boldsymbol{r}_m), \\
& \frac{\partial\overline{\omega}}{\partial t} + \nabla\cdot(\boldsymbol{u}\overline{\omega} + Pr\nabla\overline{\omega}) = \overline{\psi}, \\
& \nabla^2\overline{\psi} = \frac{\partial(T,\overline{T})}{\partial(x,y)} + \frac{\partial(\omega,\overline{\omega})}{\partial(x,y)}.
\end{aligned} \qquad (19)
$$

For many sensors, the right-hand side of the adjoint temperature equation is equal to the sum of each sensor's contribution $(T - T_m)$. As only one term remains on the right-hand side of Eq. (17), it follows, by comparison with Eq. (8), that the gradient of the objective functional is equal to the adjoint temperature at the surface where the unknown flux is being sought, that is $\nabla E = \overline{T}$. This holds true in general for an arbitrary flux $q(C^*,t)$. For a flux that is a function of t only, the gradient then corresponds to the average value of the adjoint temperature over the active surface C^*.

It should be noted that to solve the adjoint equation with the "end condition" at the physical time $t = t_f$, one should first proceed with the change of variable $\tau = t_f - t$. Via this transformation, the adjoint problem becomes an initial value problem in τ.

3. Method of conjugate gradient

The overall CG algorithm may be summarized as follows [5,27,29]:

1. Set initial conditions and choose initial guess q^0. Set iteration counter $k = 0$.
2. Solve the direct problem with q^k to obtain T^k.

3. Evaluate the error $T^k - T_m$ at the sensors position(s).
4. Solve the adjoint problem backward in time to obtain $\overline{T}^k$.
5. Evaluate the gradient $\nabla E^k = \overline{T}^k(C^*, t)$.
6. Calculate the search direction p^k. If $k = 0$, $p^k = -\nabla E^k$, otherwise, $p^k = -\nabla E^k + \gamma^k p^{k-1}$ with

$$\gamma^k = \frac{\langle \nabla E^k - \nabla E^{k-1} | \nabla E^k \rangle}{\|\nabla E^{k-1}\|^2}.$$

7. Solve the sensitivity problem with $\Delta q = p^k$ on boundary C^* to obtain $\tilde{T}^k$ at the sensor's position.
8. Calculate the step size

$$\alpha^k = -\frac{\langle T^k - T_m | \tilde{T}^k \rangle}{\|\tilde{T}^k\|^2}.$$

9. Update to $q^{k+1} = q^k + \alpha^k p^k$.

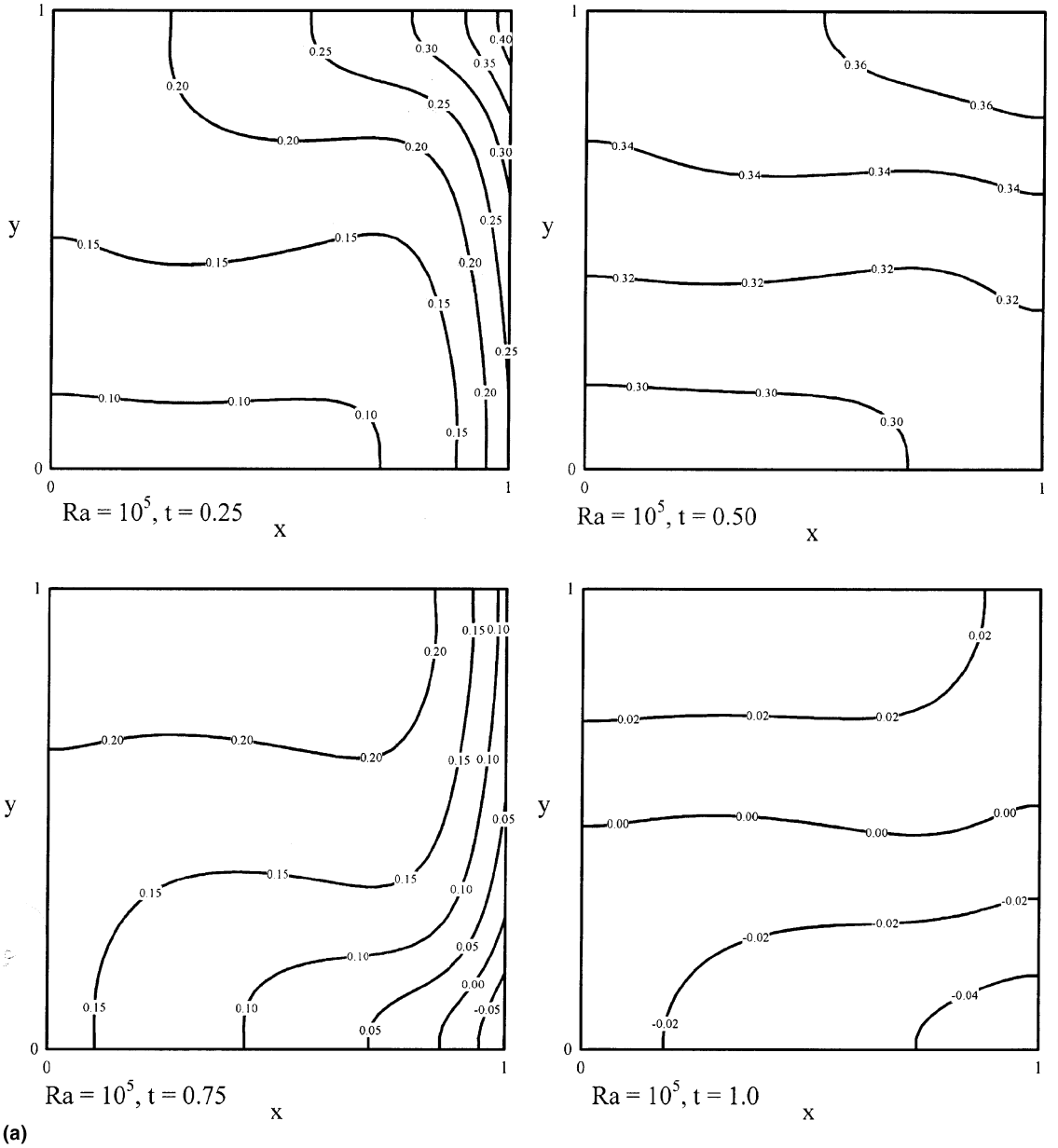

Fig. 4. (a) Isotherms, direct problem, $q(t) = -\sin(2\pi t)$, $Ra = 10^5$; (b) streamlines, direct problem, $q(t) = -\sin(2\pi t)$, $Ra = 10^5$.

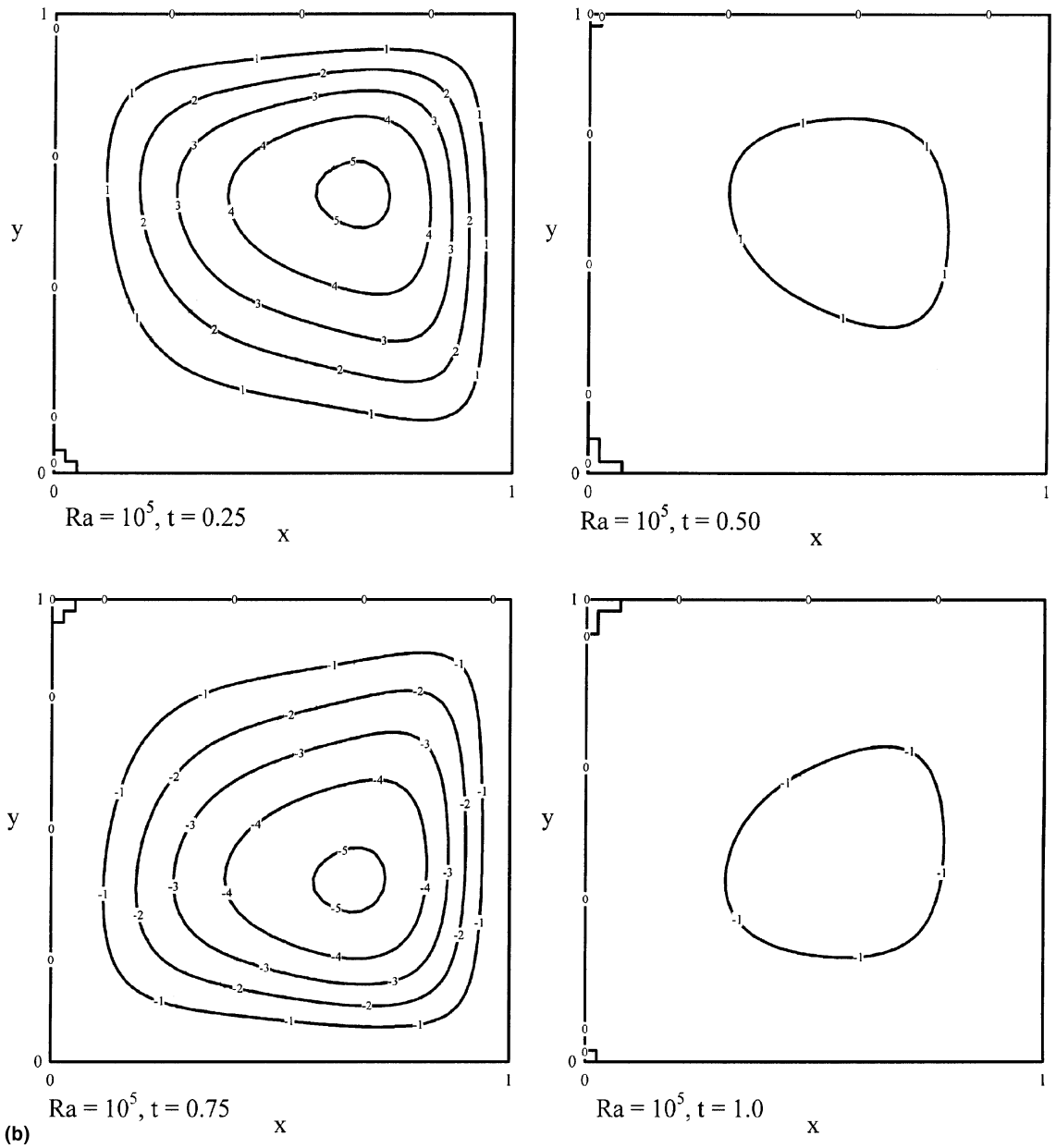

Fig. 4 (*continued*)

10. Set $k \leftarrow k+1$, go back to step 2, repeat until convergence criterion $E^k < \varepsilon E^0$ is satisfied.

The errors $E^0, E^1, \ldots E^n$ are defined from Eq. (4) with T obtained from q^n. The discrepancy principle [16,19,23] was used here to select a value for ε when the temperature data contain random errors with uniform distribution. Assuming that $T^n - T_m \approx \sigma T_m$ where σ is the standard deviation of the measurements, which is taken as a known constant, the stopping criterion expression $\varepsilon = \sigma^2 t_f$ follows from Eq. (4). Nevertheless, some results are presented for computations going beyond this limit to demonstrate the effect of noise in the data. For exact data, the stopping criterion was set at $\varepsilon = 2.510^{-6}$ or computations were stopped at the 20th iteration if the criterion had not been reached already.

4. Results and discussion

Numerical solutions to the sets of direct, sensitivity and adjoint equations for a square cavity with adiabatic top and bottom walls sketched in Fig. 1(b), are obtained

by the control volume method, with a time step $\Delta t = \Delta\tau = 10^{-2}$ and a 41×41 uniform mesh. All the computations start from $q^0 = 0$ as initial guess for the flux, for a simulation time $t_f = 1$. Since the adjoint temperature field is zero at the final time t_f, the conjugate direction vanishes also and the estimated value of the flux at t_f is always equal to the initial guess value. Although the conjugate gradient method can be modified to alleviate this difficulty [23], it is not the main purpose of this study to examine the inverse solution at t_f. The discussion will be restricted to fluxes which are zero at t_f and focus on the effects of convection on the convergence of the algorithm, by comparison with the results obtained in the case of pure conduction, i.e., when $Ra = 0$.

Inverse solutions are first obtained from exact simulated data. Effects of random errors will be considered next. In order to analyze the effects of Rayleigh number, sensor's position and different types of boundary conditions, numerical solutions are presented for the cases shown in Table 1.

4.1. Effects of Rayleigh number and sensor's position

4.1.1. Conduction regime

Results obtained for the inverse conduction problem using the CG method were presented in a recent paper by Prud'homme and Nguyen [30]. It was then shown from a Fourier analysis that the convergence speed of the inverse solution slows down as frequency increases. As a consequence, the multiple frequency components of an arbitrary flux will not be reproduced all at the same time by the CG algorithm, but one after the other, beginning with the lowest frequency and proceeding successively to the highest. This sequential convergence process is at the heart of the regularization power of the method. This feature allows for instance the satisfactory prediction of an unknown flux from noisy temperature data, by stopping the iteration process before the undesirable components of the noise are recovered.

Let us first reproduce a time-dependent heat flux of the form $q = \sin(2\pi t)$ with a sensor located on the left boundary, i.e., at $x = 0$. The temperature field obtained by solving the direct problem with this boundary heat flux is shown in Fig. 2(a). The heat flux predicted by solving the inverse problem is shown in Fig. 2(b). The inverse solutions obtained with a sensor located at $x = 0$ and $x = 0.5$, respectively, are presented together with the exact heat flux. This figure clearly shows that the CG algorithm can predict an unknown heat flux of the form $q = \sin(2\pi t)$, with a single sensor located at $x = 0$.

4.1.2. Weak convection regime

For $Ra = 10^3$, computation shows that convection is still very weak inside the cavity. The shape of the isotherms remains therefore close to the uniform pattern of the pure conduction regime. Consequently, the heat flux can still be recovered with a single sensor located at $x = 0$ as before.

4.1.3. Moderate convection regime

For $Ra = 10^4$, the influence of convection now becomes significant, as can be seen in Fig. 3(a) and (b), which show, respectively, the isotherms and streamlines obtained using $q = \sin(2\pi t)$ as before. The inverse solution obtained with a sensor located at $x = 0$ is not as

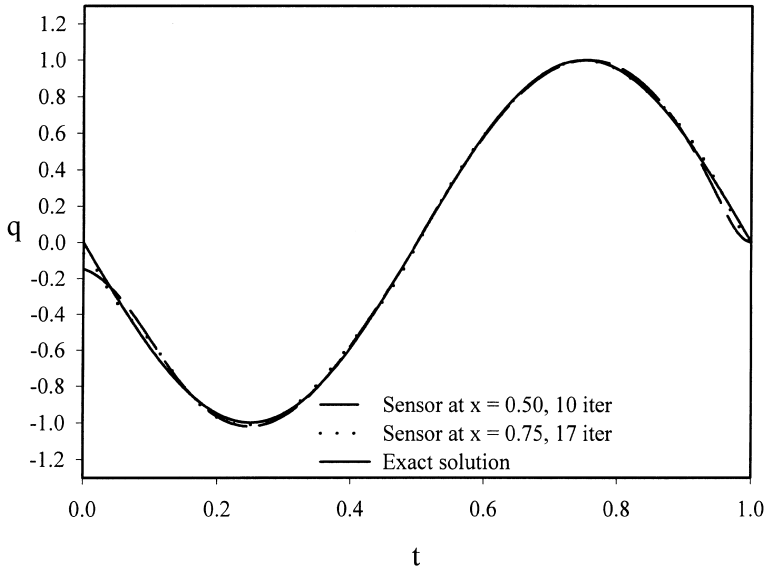

Fig. 5. Flux prediction, $q(t) = -\sin(2\pi t)$, $Ra = 10^5$.

good here as in the weak convection case. Satisfactory results can be achieved by taking the sensor closer to the active boundary, for example, at $x = 0.25$ or $x = 0.75$, as shown in Fig. 3(c).

4.1.4. Strong convection regime

By increasing the Rayleigh number to still higher levels, convection becomes strong enough for thermal boundary layers to form along the cavity walls, as can be seen in Fig. 4, where the streamlines and isotherms obtained at $Ra = 10^5$ are drawn. It appears by comparison with Fig. 2(a) that there is now a definite stratification over most of the cavity, and that the boundary layer is intermittent, which reveals a fairly complex temperature field behavior. In order to get a satisfactory solution, the sensors must be moved closer to the active boundary. The inverse solutions obtained with a single sensor located at $x = 0.50$ and $x = 0.75$, respectively, are plotted in Fig. 5. As the sensitivity is greater for a sensor placed at $x = 0.75$ than for a sensor located at $x = 0.50$, the predicted flux profile is more accurate over the time interval of the simulation.

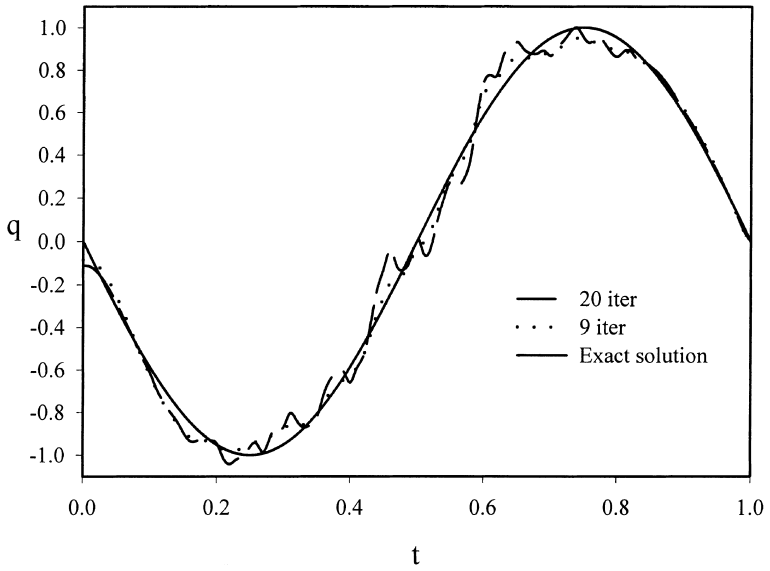

Fig. 6. Flux prediction, noisy data, $q(t) = -\sin(2\pi t)$, $Ra = 10^4$, sensor at $x = 0.75$, $\sigma = 0.04$.

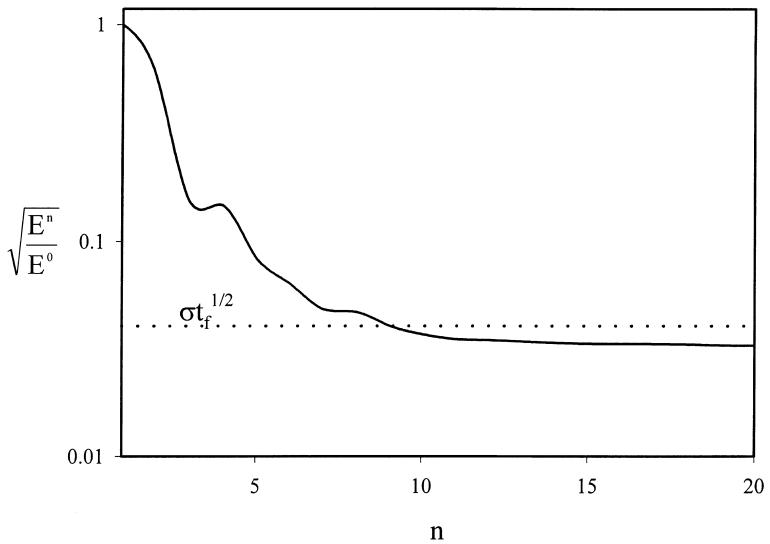

Fig. 7. Relative error, noisy data, $q(t) = -\sin(2\pi t)$, $Ra = 10^4$, sensor at $x = 0.75$, $\sigma = 0.04$.

4.2. Effects of random errors

When inverse problems are solved using noisy data, the iterative regularization effect of the CG algorithm on the solution can be detected just as well as in conduction, and used with much profit to optimize the final result. Fig. 6 clearly proves the point, by presenting a reasonably accurate solution obtained after 9 iterations, using the stopping criterion $\varepsilon = \sigma^2 t_f$. The solution obtained after 20 iterations, when the high frequency components of the noises embedded in the data are recovered, appears far less satisfactory in comparison. Although the optimal number of iterations is difficult to determine a priori, the plot of the relative error represented in Fig. 7 confirms the validity of the discrepancy principle, suggesting an optimal number of iterations between 7 and 10, roughly. To give a more complete description of the convergence process, Fig. 8 presents the solution obtained after each of the first 4 iterations.

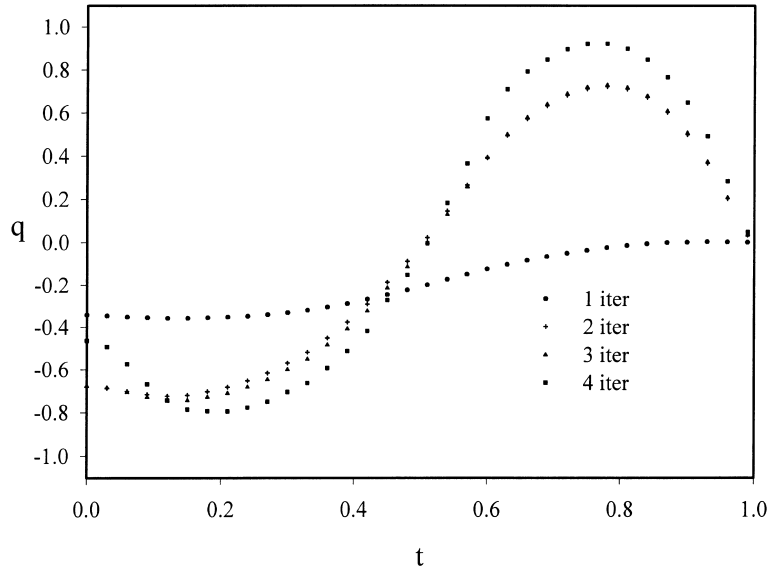

Fig. 8. Early solutions, noisy data, $q(t) = -\sin(2\pi t)$, $Ra = 10^4$, sensor at $x = 0.75$, $\sigma = 0.04$.

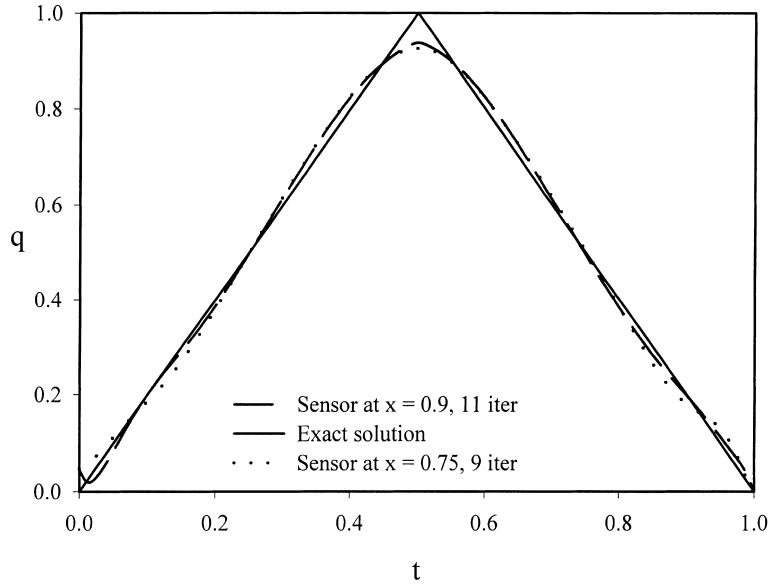

Fig. 9. Flux prediction, triangular profile, $Ra = 10^5$.

4.3. Effects of boundary conditions

We now consider two other typical heat flux profiles on the active boundary, namely, the triangular and step function profiles depicted in Figs. 9 and 10, respectively. Satisfactory results can be achieved at $Ra = 10^5$ with a single sensor located at $x = 0.90$ in both cases, and also with a sensor located at $x = 0.75$ for the triangular profile. As could be expected, the triangular flux, with Fourier coefficients inversely proportional to n^2, can be recovered more easily than the step flux, with Fourier coefficients inversely proportional to n. The consequence of recovering only so many components of the series of both fluxes with the CG method, equivalent to a truncation of their Fourier series, is therefore more visible for the step function.

It is worth noting that hitherto, we considered only fluxes which were a priori time dependent. In fact, without any prior knowledge that q is only a function of time, one should look for q as a function of both time

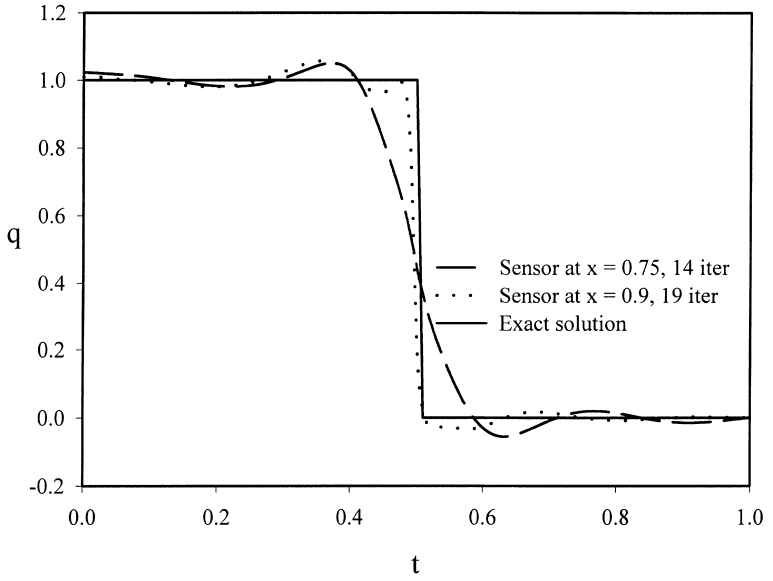

Fig. 10. Flux prediction, step profile, $Ra = 10^5$.

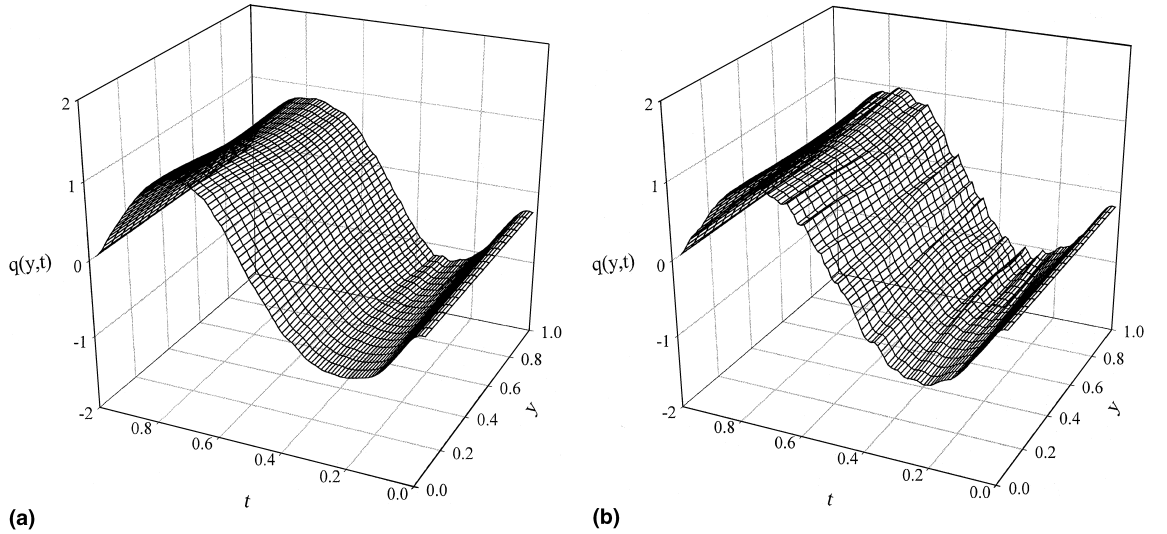

Fig. 11. (a) Flux prediction, noisy data, $q(t) = -\sin(2\pi t)$, 9 iterations, $Ra = 10^4$, 19 sensors at $x = 0.75$, $\sigma = 0.04$; (b) flux prediction, noisy data, $q(t) = -\sin(2\pi t)$, 20 iterations, $Ra = 10^4$, 19 sensors at $x = 0.75$, $\sigma = 0.04$.

and space, i.e., $q = q(y,t)$, by using as many sensors as there are grid points in the y-direction. The prediction of $q = \sin(2\pi t)$ from noisy data with sensors located at $x = 0.75$, after 9 and 20 iterations are shown in Figs. 11(a) and (b), respectively. It is noticed from the figure that the solutions are no longer perfectly uniform along y, since they are built from the local values of the adjoint temperature over the active boundary instead of the average values used for the profiles plotted in Fig. 6.

A case where the unknown heat flux depends on both space and time can be considered. We thus try to recover the solution $q = \sin(2\pi t)\sin(\pi y)$ when $Ra = 10^5$. The results obtained using sensors located at $x = 0.9$ are shown in Fig. 12. Convergence is somewhat slower in this case and the shape of the profile is not predicted accurately if the sensors are placed at a larger distance $x = 0.50$ or $x = 0.75$ from the active boundary.

Finally, a very accurate prediction of the flux $q = sin(2\pi t)$ may be obtained for $Ra = 10^6$ from a sensor at $x = 0.5$, when the adiabatic boundary condition at $x = 0$ is replaced by the isothermal condition $T = 0$, as revealed in Fig. 13.

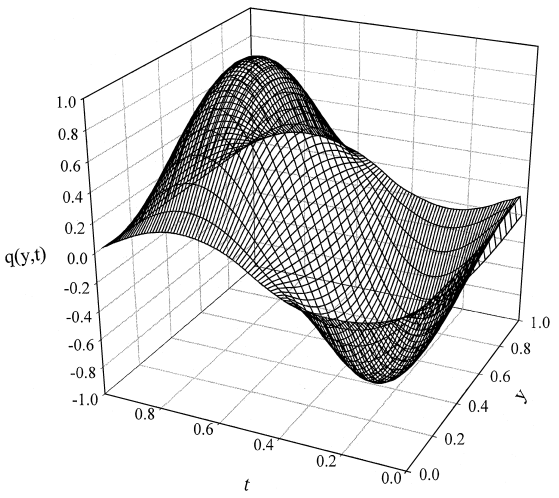

Fig. 12. Flux prediction, $q(y,t) = -\sin(2\pi t)\sin(\pi y)$, 20 iterations, $Ra = 10^5$, 19 sensors at $x = 0.90$.

5. Conclusion

Iterative solutions for the IFCP were obtained with the CG method using adjoint equations, for different types of boundary conditions and a wide range of Rayleigh numbers. Without any a priori information, the method is capable of predicting an arbitrary function $q(y,t)$ from temperatures measured by sensors located within the cavity. Stable solutions may be obtained from noisy data by stopping the iteration process before the high frequency components of the random noises start to affect significantly the inverse solution. A time-dependent heat flux can be adequately predicted with a single sensor, which must be placed closer to the active boundary as the Rayleigh number increases. The quality of the prediction is strongly dependent on the Rayleigh number and the location of the sensor, as well as on the type of conditions imposed on all the boundaries.

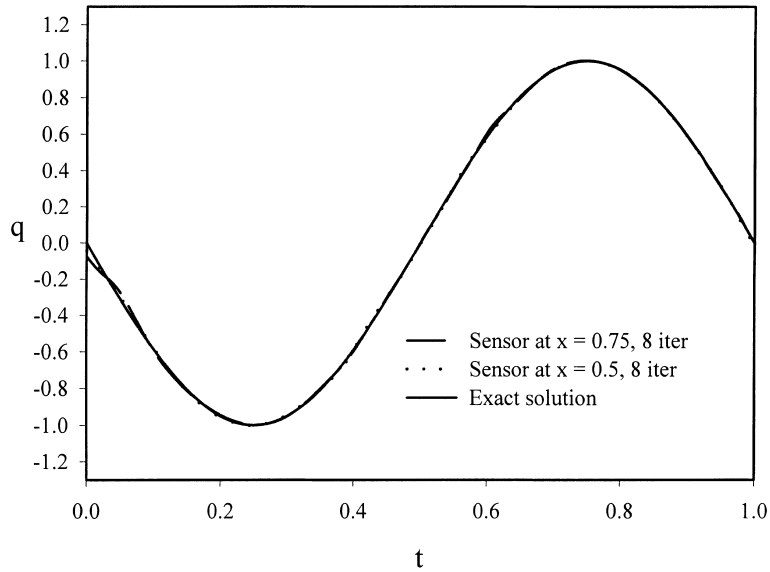

Fig. 13. Flux prediction, isothermal boundary at $x = 0$, $q(t) = -\sin(2\pi t)$, $Ra = 10^6$.

Acknowledgements

This research was supported by the Natural Sciences and Engineering Research Council of Canada.

References

[1] J. Hadamard, Lecture on Cauchy's Problem in Linear Partial Differential Equations, Yale University Press, New Haven, CT, 1923.
[2] J. Taler, W. Zima, Solution of inverse heat conduction problems using control volume approach, Int. J. Heat Mass Transfer 42 (1999) 1123–1140.
[3] C.Y. Yang, Solving the two-dimensional inverse heat source problem through the linear least-squares error method, Int. J. Heat Mass Transfer 41 (2) (1998) 393–398.
[4] A.N. Tikhonov, V.Y. Arsenin, Solutions of Ill-Posed Problems, Winston & Sons, Washington, 1977.
[5] O.M. Alifanov, Inverse Heat Transfer Problems, Springer, Berlin, 1994.
[6] F. Ramos, A. Giovannini, Résolution d'un problème inverse multidimensionnel de diffusion de la chaleur par la méthode des éléments analytiques et par le principe de l'entropie maximale, Int. J. Heat Mass Transfer 38 (1) (1995) 101–111.
[7] D.B. Ingham, Y. Yuan, Boundary element solutions of the steady state, singular, inverse heat transfer equation, Int. J. Heat Mass Transfer 37 (Suppl. 1) (1994) 273–280.
[8] D. Murio, The Mollification Method and the Numerical Solution of Ill-Posed Problems, Wiley/Interscience, New York, 1993.
[9] M. Raynaud, J. Bransier, A new finite difference method for the nonlinear inverse heat conduction problem, Numer. Heat Transfer 9 (1) (1986) 27–42.
[10] M. Raudensky, K.A. Woodbury, J. Kral, T. Brezina, Genetic algorithm in solution of inverse heat conduction problems, Numer. Heat Transfer, Part B 28 (1995) 293–306.
[11] J.V. Beck, Nonlinear estimation applied to the nonlinear inverse heat conduction problem, Int. J. Heat Mass Transfer 13 (1970) 703–716.
[12] J.V. Beck, B. Blackwell, C.R. St-Clair Jr., Inverse Heat Conduction: Ill-Posed Problems, Wiley/Interscience, New York, 1985.
[13] J. Liu, A stability analysis of Beck's procedure for inverse heat conduction problems, J. Comput. Phys. 123 (1995) 65–73.
[14] H.J. Reinhardt, A numerical method for the solution of two-dimensional inverse heat conduction problem, Int. J. Numer. Methods Eng. 32 (1991) 363–383.
[15] J.V. Beck, B. Blackwell, A. Haji-Sheikh, Comparison of some inverse heat conduction methods using experimental data, Int. J. Heat Mass Transfer 39 (17) (1996) 3649–3657.
[16] C.H. Huang, M.N. Özisik, Inverse problem of determining unknown wall heat flux in laminar flow through a parallel plate duct, Numer. Heat Transfer, Part A 21 (1992) 101–116.
[17] F.B. Liu, M.N. Özisik, Inverse analyais of transient turbulent forced convection inside parallel-plate ducts, Int. J. Heat Mass Transfer 312 (1996) 2615–2618.
[18] R. Ramanujam, Determining entrance conditions from downstream measurements, Int. Comm. Heat Mass Transfer 20 (1993) 173–183.
[19] J.C. Bokar, M.N. Özisik, An inverse analysis for estimating the time-varying inlet temperature in laminar flow inside a parallel plate duct, Int. J. Heat Mass Transfer 38 (1) (1995) 39–45.
[20] F.B. Liu, M.N. Özisik, Simultaneous estimation of thermal conductivity and heat capacity in laminar duct flow, J. Franklin Inst. B 333 (4) (1996) 583–591.
[21] P.T. Hsu, C.K. Chen, Y.T. Yang, A 2-D inverse method for simultaneous estimation of the inlet temperature and wall heat flux in a laminar circular duct flow, Numer. Heat Transfer, Part A 34 (1998) 731–745.
[22] A. Moutsoglou, An inverse convection problem, ASME J. Heat Transfer 221 (1989) 37–43.
[23] H.M. Park, O.Y. Chung, An inverse natural convection problem of estimating the strength of a heat source, Int. J. Heat Mass Transfer 42 (1999) 4259–4273.
[24] H.M. Park, W.S. Jung, The Karhunen–Loève Galerkin method for the inverse natural convection problems, Int. J. Heat Mass Transfer 44 (2001) 155–167.
[25] N. Zabaras, G. Yang, A functional optimization formulation and implementation of an inverse natural convection problem, Comput. Methods Appl. Mech. Eng. 144 (3) (1997) 245–274.
[26] G. Yang, N. Zabaras, An adjoint method for the inverse design of solidification processes with natural convection, Int. J. Numer. Methods Eng. 42 (6) (1998) 1121–1144.
[27] T.H. Nguyen, Optimization approach to the inverse convection problem, in: Proceedings of the International Worshop on Inverse Problems, HoChiMinh City, Vietnam, January 1995, pp. 83–90.
[28] M. Prud'homme, T.H Nguyen, Whole time-domain approach to the inverse natural convection problem, Numer. Heat Transfer, Part A 32 (1997) 169–186.
[29] R. Fletcher, Practical Methods of Optimization, Wiley, New York, 1987.
[30] M. Prud'homme, T.H. Nguyen, Fourier analysis of conjugate gradient method applied to inverse heat conduction problems, Int. J. Heat Mass Transfer 42 (1999) 4447–4460.